Polyoxoanion Chemistry Moves toward the Future: From Solids and Solutions to Surfaces

Walter G. Klemperer* and Craig G. Wall

Department of Chemistry, University of Illinois, 601 South Goodwin Avenue, Urbana, Illinois 61801

Received November 25, 1997 (Revised Manuscript Received December 11, 1997)

Contents

Walter Klemperer received a B.A. in Chemistry from Harvard College in 1968 and a Ph.D. in Inorganic Chemistry under the supervision of Professor F. A. Cotton from MIT in 1973. After eight years at Columbia University, he joined the faculty at the University of Illinois at Urbana−Champaign where he is currently Professor of Chemistry. His research interests include dynamic stereochemistry, polyoxoanion chemistry, metal alkoxide chemistry, and inorganic materials chemistry, including zeolite, cement, and sol–gel chemistry.

Craig G. Wall was born in Texas in 1967. He received his B.S. in chemistry from the University of Texas at Austin in 1990 and a Ph.D. in 1995 from the University of North Carolina where he studied electron-transfer reactions in synthetic peptides under the direction of Professors Bruce W. Erickson and Thomas J. Meyer. He is currently a postdoctoral fellow at the University of Illinois with Professor Walter G. Klemperper where he using scanning tunneling microscopy to investigate self-assembled inorganic monolayers.

I. Introduction

Early transition metal polyoxoanion chemistry has developed rapidly during the past 25 years, and much of the progress achieved can be attributed to parallel advances in analytical instrumentation. For example, fewer than 15 structure types were known for early transition metal polyoxoanions in 1970.[1] Since then, the widespread availability of automated X-ray diffractometers has enabled rapid solid-state structural characterization of polyoxometalates, and the number of known structure types has grown by at least an order of magnitude. The 1970s also brought commercially available NMR spectrometers with multinuclear capability, this advance allowing for rapid structural characterization in solution.[2] Progress achieved in developing the solid-state and solution chemistry of early transition metal polyoxoanions has not been matched, however, by a corresponding development of their surface chemistry. The reason for this state of affairs is quite simple: surface analytical techniques corresponding to those available for structural characterization in solution and in the solid state have only very recently become available.

Early transition metal polyoxoanions have long been known to have an extensive surface chemistry that plays a key role in such traditional areas as catalysis,[3] corrosion protection,[4] and electrochemistry,[5] as well as newer areas such as metal colloid stabilization,[6] electroless deposition,[7] bilayer lithography,[8] and fine metallic patterning.[9] The precise role played by polyoxoanions at solid−gas, solid−solid, and solid−liquid interfaces in these systems has been difficult to establish, however, in the absence of structural information on the atomic molecular size scale. Not until 1991, when scanning probe microscopy (SPM) was applied to the study of

S0009-2665(96)00399-8 CCC: $30.00
Published on Web 01/22/1998

tungstophosphoric acid, were early transition metal polyoxoanions structurally characterized at any type of surface.[10] Since then, ordered arrays of early transition metal polyoxoanions have been structurally characterized in a variety of different surface environments using SPM techniques. This concise review treats all of these studies in an effort to define the current scope and limitations of SPM as a structural probe in polyoxoanion surface chemistry, and this treatment is followed by an assessment of future research directions. A brief introduction to SPM is also provided for those unfamiliar with the technique.

II. Scanning Probe Microscopy

The general principles of scanning probe microscopy are quite simple.[11] Ideally, an atomically sharp tip is raster scanned across the sample using a piezoelectric tip or sample holder, a feedback loop is used to maintain a constant tip−sample interaction, and the piezoelectric displacement required to maintain feedback is processed by a computer, yielding topographic and electronic information down to the angstrom size scale. In scanning tunneling microscopy (STM) the tip−sample interaction is the tunneling current, and in atomic force microscopy (AFM) the interaction is the surface force between the tip and the sample. Both techniques are experimentally challenging, since the manner in which surface features are represented is very sensitive to tip artifacts and tip shape.[12] Thermal drift is another common problem, in that thermal gradients influence the rastering of the probe tip with respect to the sample, introducing systematic discrepancies between the actual and measured surface geometry.[13] Other artifacts can be introduced by excessively filtering the raw data, leading to unreliable conclusions about topographical or electronic features of the sample.

In the case of STM, an electric potential (bias) is first applied between a very sharp metal tip and a conducting sample. The tip is then brought to within a few angstroms of the surface, allowing a tunneling current to flow. Theoretically, this is achieved before mechanical point contact is reached between the tip and sample. A feedback loop is activated to maintain a specified tunneling current and the topography observed is defined by the sample−tip separation required to sustain constant tunneling current. Localized electronic states can also be examined by positioning the tip at a given location and a fixed tip−sample separation and measuring the voltage dependence of the tunneling current, an $I-V$ curve. This technique, known as tunneling spectroscopy,[14] yields curves of the type shown in Figure 1. Curve a represents the behavior observed when the tip is spatially located above a localized electronic surface state; curve b represents background current, i.e., current flowing when electrons are *not* tunneling to or from a localized surface state. The distinguishing feature of curve a is a region of negative slope referred to as negative differential resistance (NDR).

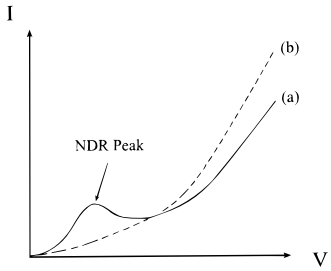

Figure 1. Schematic representation of (a) a current−voltage curve when the STM tip is spatially located above a localized electronic surface state and (b) background current when the STM tip is spatially located above a region with no localized surface states.

Tunneling current reflects the electronic states of both the tip apex and the sample surface as well as the energy dependence of the local density of states for both the sample surface and the tip apex, and detailed analysis of tunneling spectra is possible in only the simplest cases.[15] Nonetheless, qualitative comparison of local maxima in I−V curves measured from closely related systems under similar conditions can often yield useful information about the nature of localized surface states (see below).

In the case of atomic force microscopy the tip is brought into physical contact with the surface and the forces between the sample and the tip are measured by optically sensing tip deflections. Feedback is achieved by maintaining a constant force between the tip and the sample. Unlike STM, AFM is not directly influenced by the electronic structure of the sample.

III. Single Crystal Surfaces

Keïta, Nadjo, and Kjoller were the first to examine surfaces of crystalline polyoxoanion salts on a molecular level using SPM techniques.[16] Single crystals of $Na_6H_2CeW_{10}O_{36}\cdot 30H_2O$ were examined with atomic force microscopy (AFM) in an effort to resolve $[CeW_{10}O_{36}]^{8-}$ anions having the structure shown in Figure 2a,b. Raw images (see Figure 3a) yielded periodic patterns of the type shown in Figure 3b,c after Fourier filtering.[16,17] Since the observed nearest-neighbor separations of 12−13 Å correspond to nearest-neighbor $CeW_{10}O_{36}^{8-}$ anion separations in crystalline $Na_6H_2CeW_{10}O_{36}\cdot 30H_2O$,[18] the features observed by AFM were assigned to individual $CeW_{10}O_{36}^{8-}$ anions. This assignment was reinforced by comparison of AFM images with the arrangement of $CeW_{10}O_{36}^{8-}$ anions on the (010) face of crystalline $Na_6H_2CeW_{10}O_{36}\cdot 30H_2O$ as shown in Figure 4a. Unit cell parameters determined X-ray crystallographically ($a = 18.14$ Å $b = 18.62$ Å, $c = 18.51$ Å, and $\beta = 95.9°$) showed good agreement with parameters measured from AFM images ($a = 18.0 \pm 0.5$ Å $c = 18.3 \pm 0.5$ Å, and $\beta = 96 \pm 5°$). The authors treated this assignment as tentative, however, since uncertainties in unit cell parameters determined by AFM do not allow for unambiguous discrimination between unit cell parameters on the (100), (010), and (001) faces.

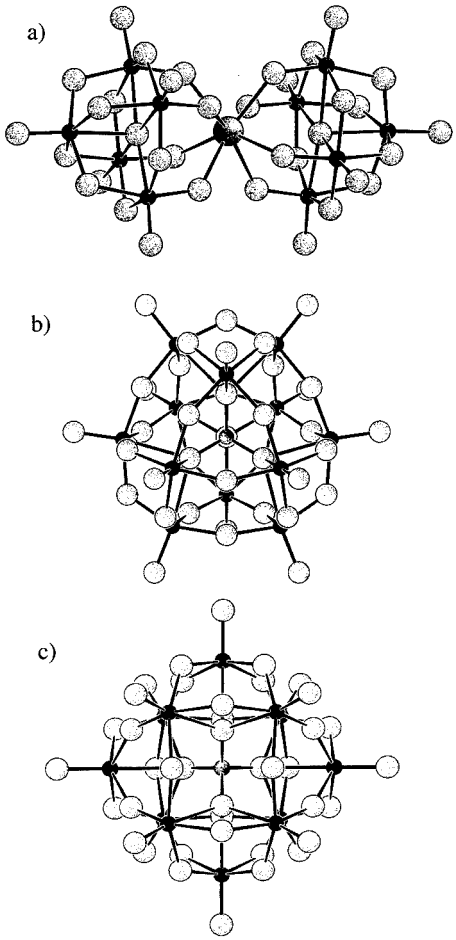

Figure 2. Structures of selected polyoxoanions discussed in the text. A ball-and-stick model of the $CeW_{10}O_{36}^{8-}$ anion in $Na_6H_2CeW_{10}O_{36}\cdot 30H_2O$[18] is shown in a, where the tungsten atoms are represented by small, filled circles; oxygen atoms, by medium-sized, shaded circles; and the cerium atom, by a large, shaded circle. Ball-and-stick models of the $PW_{12}O_{40}^{3-}$ anion in $[H_5O_2]_3PW_{12}O_{40}$[20] viewed b along a 3-fold rotational symmetry axis and c along a 2-fold rotational symmetry axis of the T_d-symmetric molecular ion. The phosphorus atom is represented by a small, shaded circle; the remaining atoms are represented as in a. Other $XM_{12}O_{40}^{n-}$ anions discussed in the text have the same Keggin structure shown in b and c.

IV. Evaporative Solution Deposition on Graphite

To achieve higher heterogeneous catalytic activity, polyoxoanion catalysts are often supported on high surface area materials, and in many cases, the intrinsic reactivity of the polyanion is modified through interaction with the support.[3] The nature of the polyoxoanion−support interaction is therefore of interest, and since carbon is a common support material, the direct observation of polyoxoanions on carbon materials has been the objective of several studies. In each case, samples have been prepared by evaporative solution deposition on highly oriented pyrolytic graphite (HOPG). This technique, sometimes referred to as solvent-casting, involves placing a drop of a polyoxoanion salt solution on an HOPG surface and simply allowing the solvent to evaporate to dryness. This results in the crystallization of the polyoxoanion salt on the graphite surface: a polycrystalline "rind" appears around the perimeter of the original liquid drop, enclosing an area where a thinner polyoxoanion salt film is formed.[19]

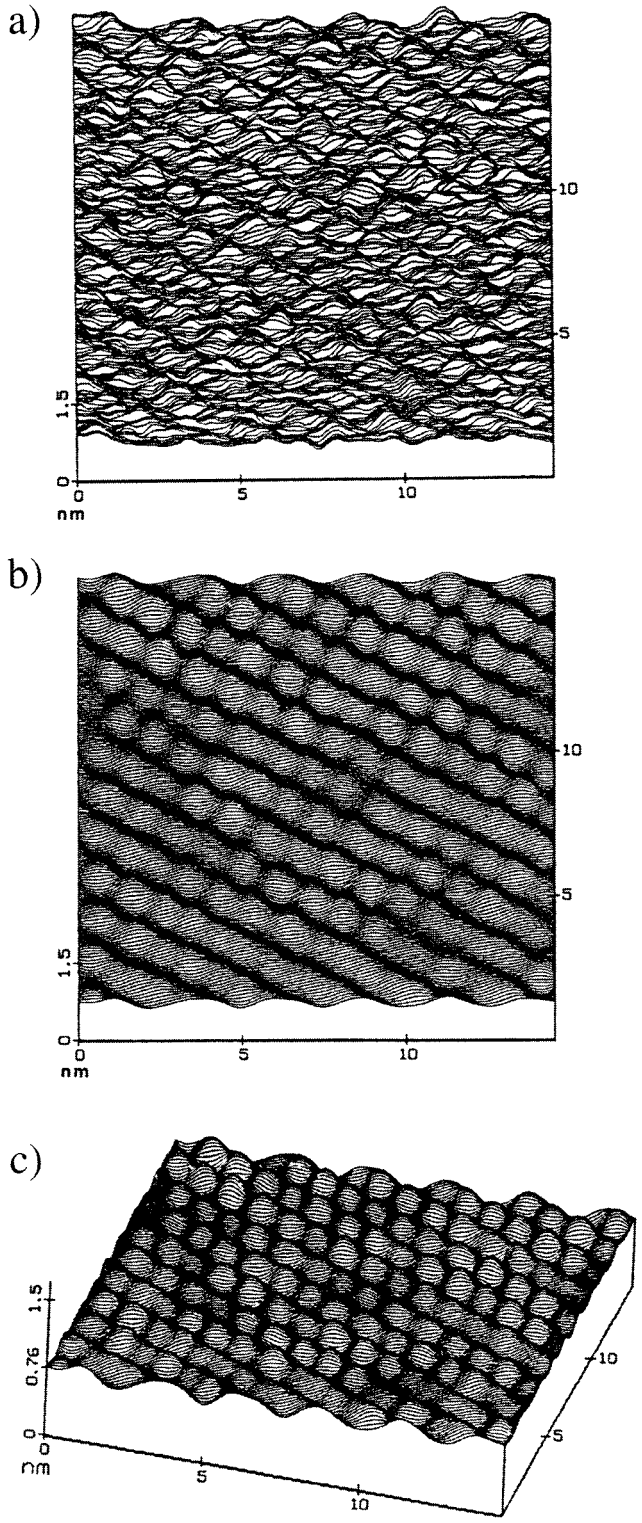

Figure 3. (a) Line plot AFM image of a sodium decatungstocerate(IV) single-crystal surface in air at room temperature (raw data). (b) Image shown in a after fast-Fourier transform (FFT) filtering. (c) Perspective view of the AFM image shown in b. (Reprinted with permission from ref 17. Copyright 1992 Elsevier Science.)

Keïta and Nadjo were the first to demonstrate that polyoxometalates deposited on HOPG by solvent-casting could be imaged by STM.[10] As shown in

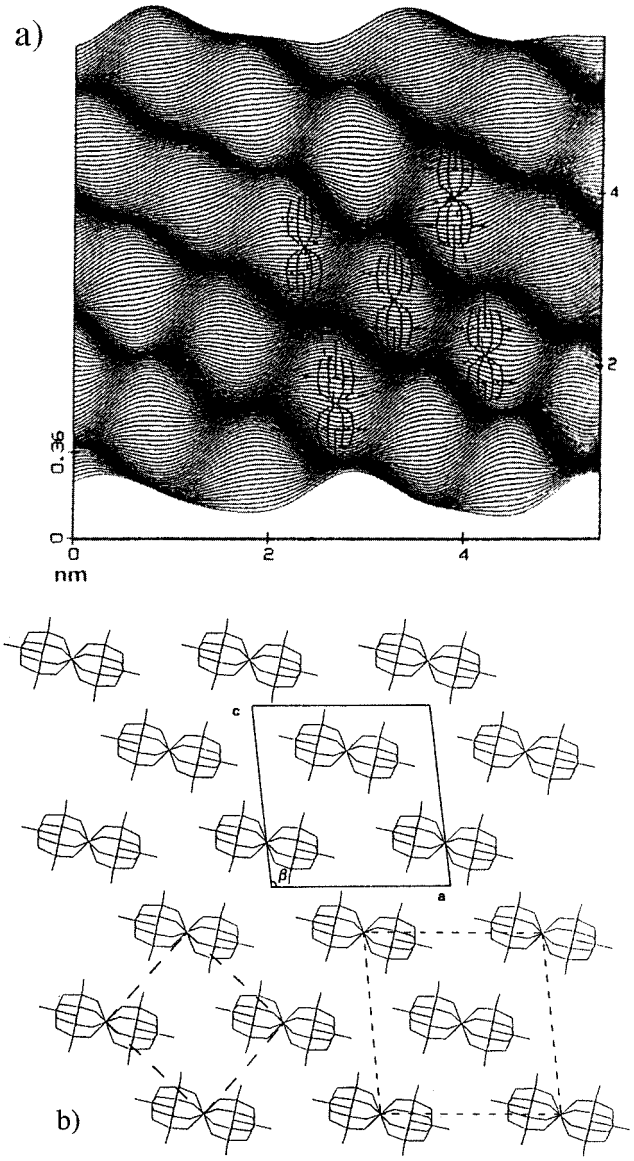

Figure 4. (a) FFT filtered line plot AFM image of a sodium decatungstocerate(IV) single crystal in air at room temperature with a wire scale model of the anion arrangement on the (010) crystal surface superimposed. (b) Wire model of the $CeW_{10}O_{36}^{8-}$ anion arrangement on the (010) crystal surface. In b, solid lines outline the projection of the crystallographic[18] unit cell projected onto the *ac* plane, and dotted lines outline the primitive (left) and centered (right) two-dimensional unit cells of the crystallographic anion arrangement projected on the (010) plane. (Reprinted with permission from ref 16. Copyright 1991 Elsevier Science.)

Figure 5, Fourier-filtered images of the phosphotungstic acid $H_3PW_{12}O_{40}$ on HOPG displayed a quasi-hexagonal arrangement of features separated by about 10 Å. The authors noted that this distance approximates the 10−11 Å diameter of the T_d-symmetric $PW_{12}O_{40}^{3-}$ heteropolyanion[20] shown in Figure 2b,c and therefore assigned these features to the anion. Observation of individual anions was rationalized in terms of the electronic structure of early transition metal polyoxoanions, where the valence band composed of HOMO's has predominantly oxygen p character and the conduction band composed of LUMO's has predominantly metal d character.[21] Tunneling of electrons to and from the

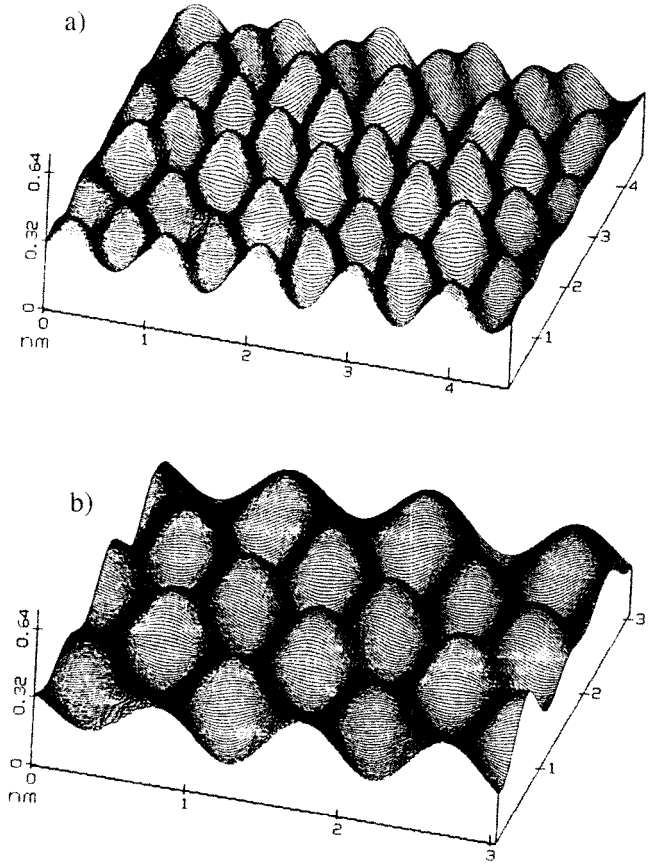

Figure 5. FFT-filtered STM images of $H_3PW_{12}O_{40}$ deposited on graphite, measured in air at room temperature: (a) 4.5 × 4.5 nm^2 image; (b) 3.0 × 3.0 nm^2 region of image shown in a. (Reprinted with permission from ref 10. Copyright 1991 Elsevier Science.)

STM tip therefore involves electronic states localized largely on the polyoxotungstate tungsten centers. Electron transfer from the graphite surface to the sample−tip interface presents no problem since polyoxotungstates are known have semiconducting properties in the solid state.[22]

To provide independent support for their interpretation of STM images of phosphotungstic acid deposited on HOPG by solvent-casting, Keïta and co-workers next studied $Na_6H_2CeW_{10}O_{36}$ deposited on HOPG by solvent evaporation.[17] Although the STM images obtained showed little or no ordering, the surface features observed showed dimensions of about 17 Å, a value consistent with dimensions of $[CeW_{10}O_{36}]^{8-}$ anions in $Na_6H_2CeW_{10}O_{36}\cdot 30H_2O$ obtained from AFM[16] and X-ray crystallographic[18] studies.

Tunneling spectroscopic studies reported by Barteau and co-workers have also provided strong evidence that STM images of early transition metal polyoxoanions deposited on HOPG by solvent evaporation derive from surface states involving metal d orbitals. Initial studies of solvent cast $H_3PMo_{12}O_{40}$, $Na_4SiW_{12}O_{40}$, $H_7SiW_9V_3O_{40}$, and $(NH_4)_6V_{10}O_{28}$ films showed patterns having 10−12 Å periodicities consistent with molecular dimensions determined X-ray crystallographically (see Figure 6).[23] For the two polyvanadate complexes, $I-V$ curves obtained when the STM tip was positioned over surface features

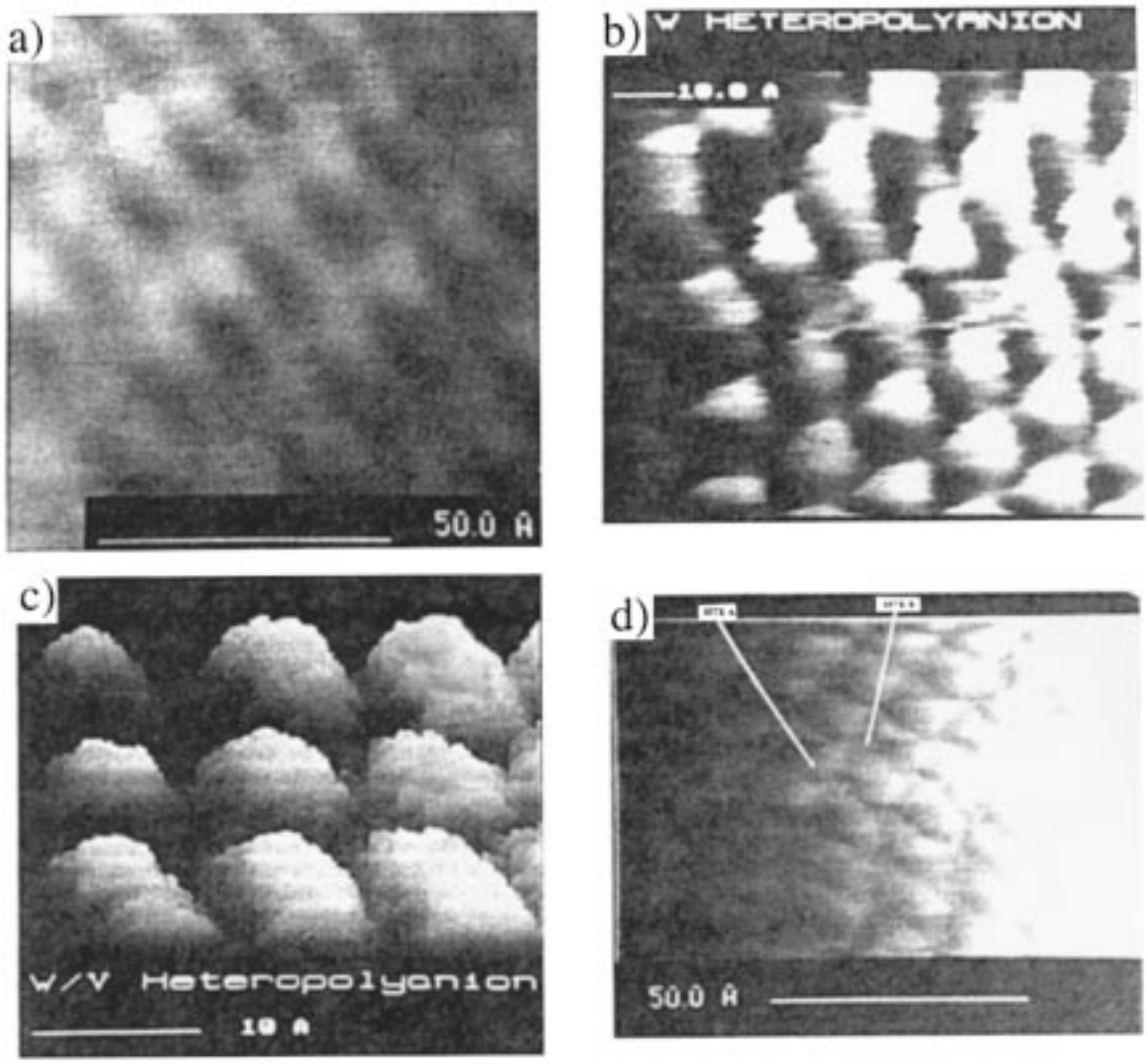

Figure 6. Low-pass filtered STM images of (a) $H_3PMo_{12}O_{40}$, (b) $Na_4SiW_{12}O_{40}$, (c) $H_7SiW_9V_3O_{40}$, and (d) $(NH_4)_6V_{10}O_{28}$ deposited on graphite. (Reprinted from ref 23. Copyright 1992 American Chemical Society.)

showed NDR behavior, and curves obtained at interstitial sites showed normal background behavior (see Figure 1). NDR peaks appeared at a positive potential for $H_7SiW_9V_3O_{40}$ and a negative potential for $(NH_4)_6V_{10}O_{28}$, reflecting the greater reducibility of $H_7SiW_9V_3O_{40}$. These STM imaging and tunneling spectroscopic studies have been extended to include further salts of the phosphomolybdate ion $[PMo_{12}O_{40}]^{3-}$ (see Figure 2b,c) and its metal-substituted derivatives: $H_3PMo_{12}O_{40}$,[19] $H_4PMo_{11}VO_{40}$,[19] $H_8PMo_{10}VCuO_{40}$,[19] $K_3PMo_{12}O_{40}$,[19] $H_{3-x}Cs_xPMo_{12}O_{40}$ (x = 1, 2, 2.5, 3),[19] $H_3PMo_{12}O_{40}\cdot n$py (py = pyridine),[24] $Cs_3PMo_{12}O_{40}$,[24] $H_{3-x}Cu_{x/2}PMo_{12}O_{40}$ (x = 1, 2, 3),[25] $Mg_{3/2}PMo_{12}O_{40}$,[25] $BiPMo_{12}O_{40}$,[25] and $H_3PMo_xW_{12-x}O_{40}$ (x = 0, 3, 6, 9, 12).[26] Tunneling spectra showed the same features observed in earlier studies: NDR curves when the tip was positioned over surface features and background current when the tip was positioned over interstices between these features. As was the case in the earlier studies, NDR peaks for the more reducible, i.e., more strongly oxidizing, compounds appeared at less negative tip potentials. Representative STM images are shown in Figures 7 and 8.

There is general agreement in all of the studies cited above that evaporative solution deposition of early transition metal polyoxoanions onto HOPG yields ordered two-dimensional arrays of polyoxoanions on the HOPG surface and that the features observed in STM images of these surfaces derive from electrons tunneling to and from localized surface states associated with the conduction band of the polyoxoanions. Beyond these two statements, however, little can be claimed with any degree of certainty concerning the nature of the ordered arrays formed. No measurements of the polyoxoanion film thickness have been reported, and claims of monolayer formation have been supported only by tunneling spectroscopy.[19,23−26] Unfortunately, tunneling spectra display only the standard NDR peaks normally associated with localized states on semiconductor surfaces, and such features are equally consistent with monolayers and multilayers on HOPG. In-plane nearest-neighbor separations between polyoxoanions *have* been measured, but interpretation of these distances is ambiguous.[27] For example, the STM image of "pyridine-exposed" $H_3PMo_{12}O_{40}$ shown in Figure 8 has been assigned to an oblique monolayer

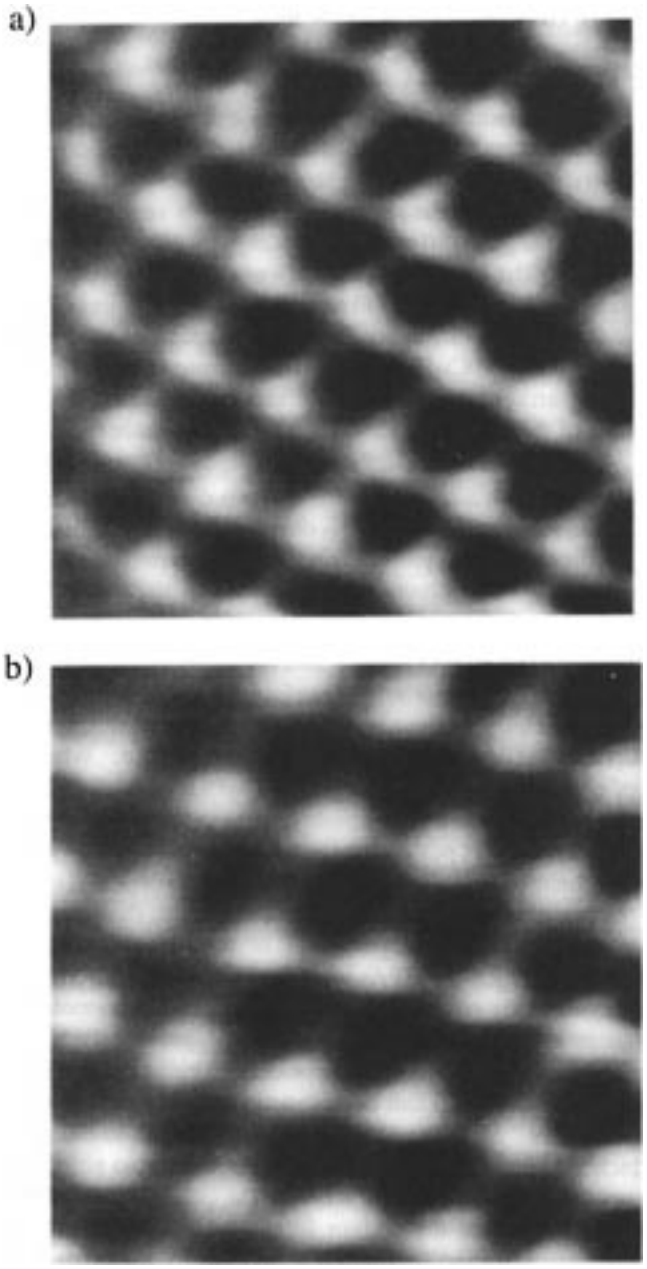

Figure 7. STM images of (a) $H_3PMo_{12}O_{40}$ (5.07 × 5.07 nm^2) and (b) $Cs_3PMo_{12}O_{40}$ (7.0 × 7.0 nm^2) on HOPG. Both samples were prepared by evaporative solution deposition. (Reprinted from ref 19. Copyright 1996 American Chemical Society.)

of $[PMo_{12}O_{40}]^{3-}$ anions separated by pyridinium $[C_5H_5NH]^+$ cations. Given, however, its relatively small deviation from hexagonal symmetry, the STM image could equally well derive from a crystalline multilayer where $[PMo_{12}O_{40}]^{3-}$ anions are separated by $[C_5H_5NHNC_5H_5]^+$ cations arranged in the fashion observed for $[PW_{12}O_{40}]^{3-}$ anions and $[C_5H_5NHNC_5H_5]^+$ cations on the (001) face of rhombohedral $[(C_5H_5N)_2H]_3[PW_{12}O_{40}]$.[28]

V. Electrochemical Deposition onto Graphite

Electrode surfaces modified with early transition metal polyoxoanions are proven catalysts for several electrochemical reactions.[5] Polyoxoanion-modified electrodes are prepared by electrodeposition, specifically, through application of a strongly negative electrode potential in an acidic polyoxoanion solution. STM is well-suited for in situ imaging of electrode processes,[29] and it has been applied to electrodeposition on HOPG electrodes from $(NH_4)_6[H_2W_{12}O_{40}]$[30] and $K_{10}H_3[Dy(SiMo_{11}O_{39})_2]$[31] solutions. In the case of $(NH_4)_6[H_2W_{12}O_{40}]$ electrodeposition, STM images showed ordered domains with periodicities of about 11 Å when cycling through the third reduction wave. In the case of $K_{10}H_3[Dy(SiMo_{11}O_{39})_2]$ electrodeposition, the electrodeposition was observed only if the HOPG electrode was first electrochemically pretreated in Na_2SO_4 solution, both oxidatively and reductively. Electrodeposition was effected by cycling the electrode between −0.25 and +0.50 V vs Ag/AgCl, and two different surface structures were observed by STM. Initially, a hexagonal structure was observed having a 10.6 Å periodicity. After longer deposition times, a rectangular lattice was observed with periodicities of about 10 and almost 20 Å. The STM images observed in both systems could be modeled by two-dimensional arrays of the polyoxanions present in the electrodeposition solutions, but the conditions required for electrodeposition were sufficiently drastic as to call into question the identity of the species that were actually deposited onto the electrode surface.

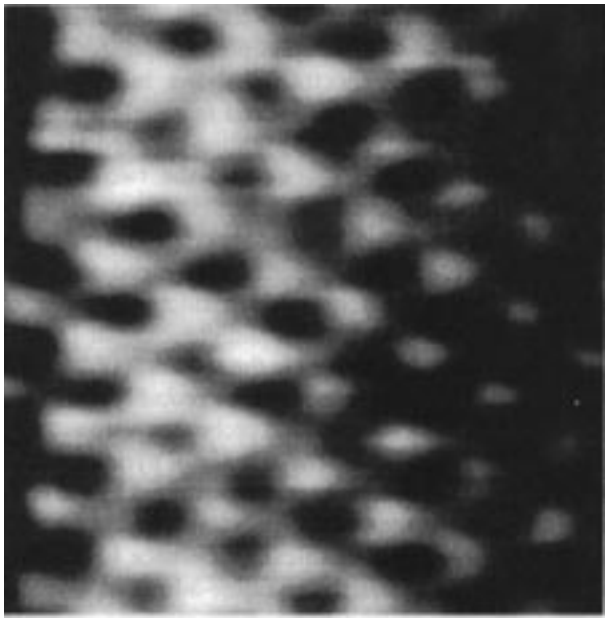

Figure 8. An 11.9 × 11.9 nm^2 STM image of $H_3PMo_{12}O_{40}$ on graphite after exposure to liquid pyridine followed by evaporation of volatiles. (Reprinted from ref 24. Copyright 1996 American Chemical Society.)

VI. Self-Assembly on Metal Surfaces

Early transition metal polyoxoanions have a strong affinity for metal surfaces, a property reflected in their efficacy as metal corrosion inhibitors.[4] This affinity has recently been exploited in the preparation of self-assembled polyoxoanion monolayers by simply immersing Ag(111) or Au(111) surfaces into acidic aqueous solutions of silicotungstic acid, $H_4SiW_{12}O_{40}$ (see Figure 2c and d).[32−34] In situ STM studies have revealed that ordered $SiW_{12}O_{40}^{4-}$ monolayers are

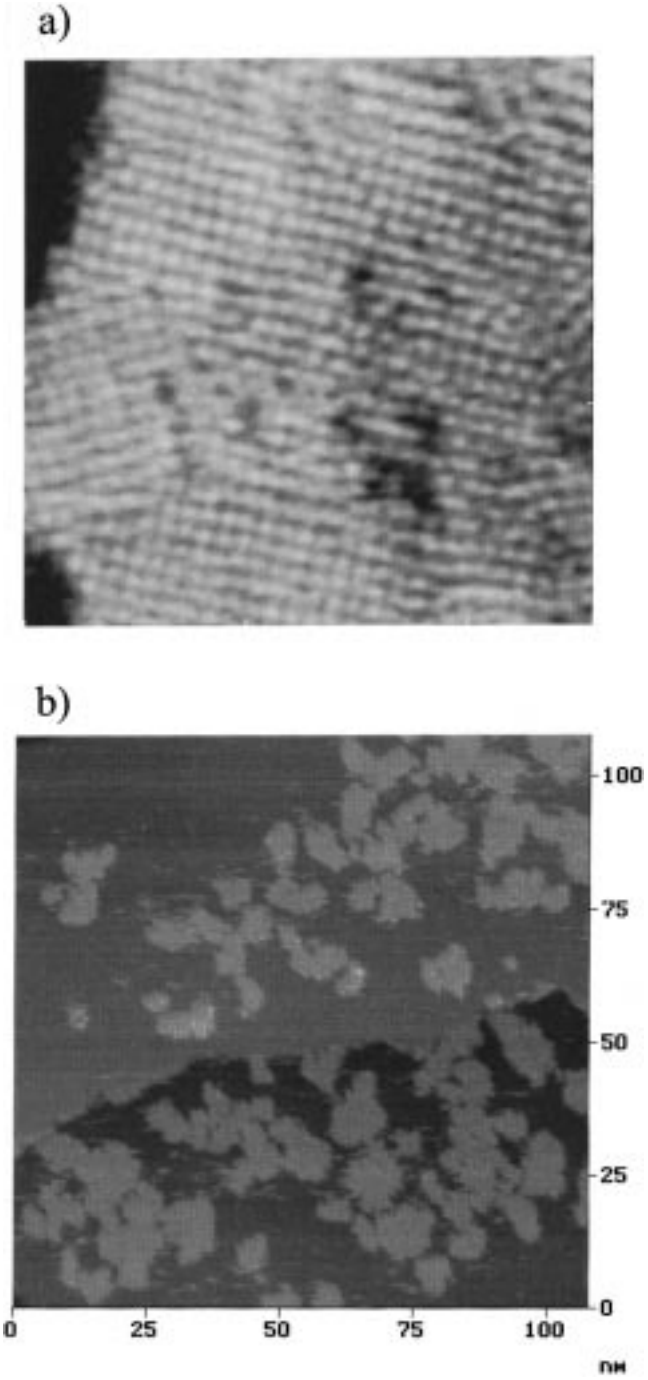

Figure 9. (a) A 28 × 28 nm^2 in situ STM image of an $SiW_{12}O_{40}^{4-}$ monolayer on Ag(111) in 0.1 M aqueous $HClO_4$. (b) A 110 × 110 nm^2 in situ STM image of a partial monolayer of $SiW_{12}O_{40}^{4-}$ on Ag(111) in 0.1 M aqueous H_2SO_4. (Reprinted from ref 32. Copyright 1996 American Chemical Society.)

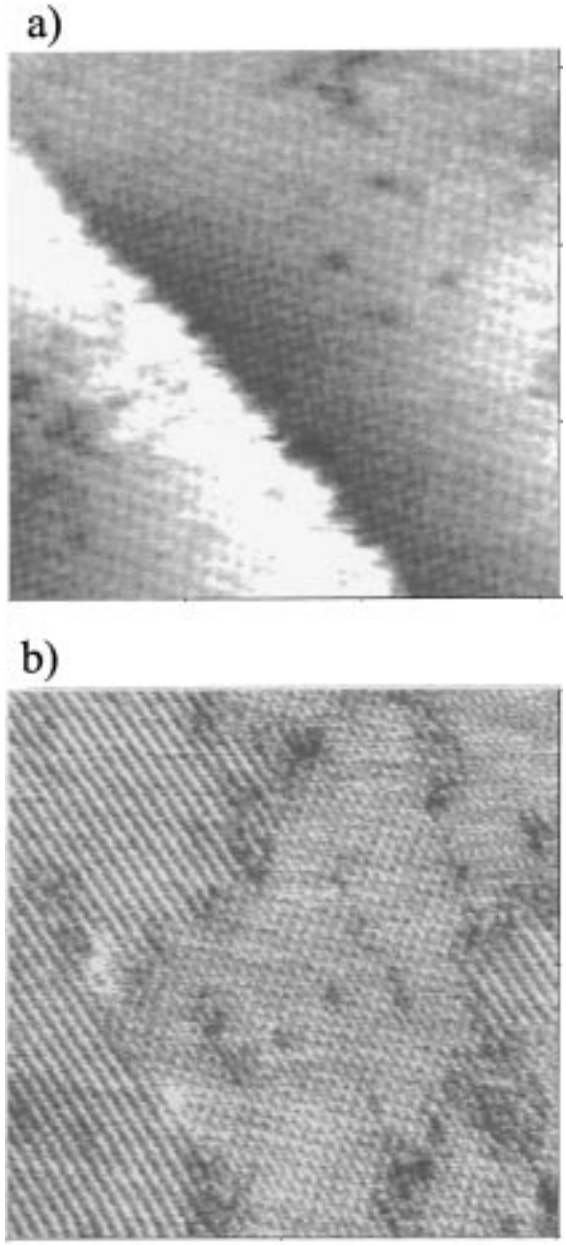

Figure 10. (a) A 31 × 31 nm^2 in situ STM image of a $SiW_{12}O_{40}^{4-}$ monolayer on Au(111) in 0.1 M aqueous H_2SO_4. (b) A 50 × 50 nm^2 in situ STM image of a $SiW_{12}O_{40}^{4-}$ monolayer on Au(111) in 0.1 M aqueous H_2SO_4. (Reprinted with permission from ref 33. Copyright 1997 Materials Research Society.)

formed spontaneously under these conditions, in the absence of an imposed potential.

An STM image of the adlattice formed by the silicotungstate ion on Ag(111) is shown in Figure 9a. This image, observed under saturation conditions, defines an approximately square lattice with a 10.2 ± 0.5 Å repeat distance. As shown in Figure 9b, islands are observed on the Ag(111) surface under conditions of partial coverage, and the islands allow the adlayer height to be estimated and established as a $SiW_{12}O_{40}^{4-}$ monolayer. Three different structures have been observed by in situ STM on Au(111) surfaces upon immersion in acidic silicotungstate solution. The image shown in Figure 10a defines an oblique lattice with 10.2 ± 0.7 and 11.8 ± 0.6 Å lattice repeats that intersect at 103 ± 4°. The two other structures are both observed in Figure 10b: a row structure with row−row separation of 11.7 ± 0.6 Å and the approximately square structure also observed on Ag(111). In the row structure, the rows are oriented parallel with a diagonal of the square structure; in the square structure, one of the sides of the square forms a 12 ± 4° angle with the one of the rows of Au(111).

The adlattices formed by the $SiW_{12}O_{40}^{4-}$ anion on Ag(111) and Au(111) surfaces, their relative orienta-

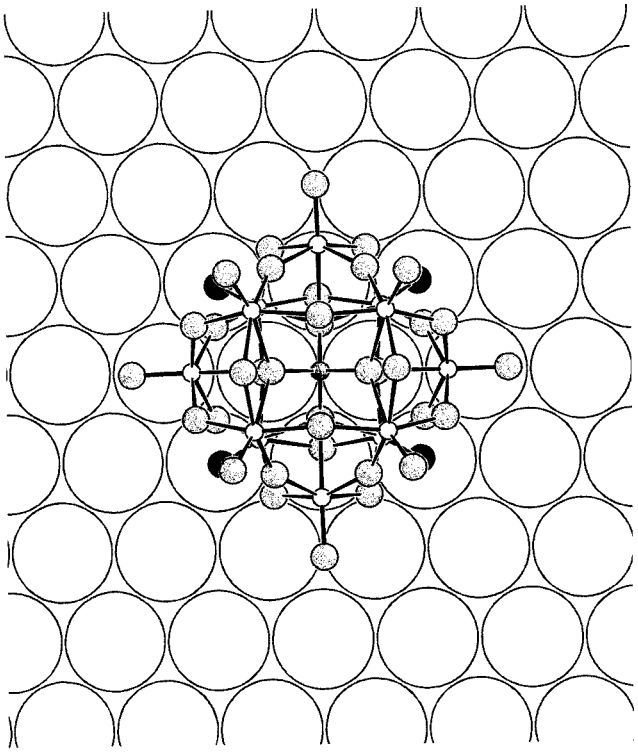

Figure 11. Proposed model of the Au(111) or Ag(111) surface interaction with the $SiW_{12}O_{40}^{4-}$ anion viewed along a C_2 axis normal to the Au surface. Note the near coincidence of the four terminally bonded oxygen atoms of the polyoxoanion (filled circles) with metal atoms on the surface (large, open circles). Tungsten atoms are represented by small, open circles; oxygen atoms, by medium-sized, shaded circles; and the phosphorus atom, by a small shaded circle. (Reprinted with permission from ref 33. Copyright 1997 Materials Research Society.)

tions, and their orientations relative to the Au(111) lattice directions can all be rationalized by a simple surface coordination model.[33,34] According to this model, the silicotungstate anion acts as a tetradentate ligand and coordinates to four metal atoms on the Ag(111) or Au(111) surface as indicated in Figure 11, where the four ligating oxygen atoms are shaded to emphasize how closely the silicotungstate "footprint" matches four atoms on the metal surface. If adlattices are generated by requiring that each silicotungstate ion be coordinated to the metal surface as shown in Figure 11 and requiring further that oxygen−oxygen between nearest neighbor silicotungstate ions not be less than 2.8 Å, the sum of two van der Waals radii for oxygen, fragments of the three most closely packed arrangements possible are shown in Figure 12. The arrangement shown in Figure 12a has diamond-shaped primitive unit cell with 10.4 Å unit cell axes intersecting at 92°; this cell is in good agreement with the "square" structures shown in Figures 9a and 10b. The arrangement shown in Figure 12b has an oblique primitive cell with 10.4 and 11.6 Å unit cell axes intersecting at 106°, in good agreement with the oblique lattice shown in Figure 12b. Finally, the structure shown in Figure 12c has a rectangular unit cell with 10.0 and 11.6 Å unit cell axes and shows good agreement with the row structure shown in Figure 10b. The following relations hold between these unit cells and the Au(111) rows

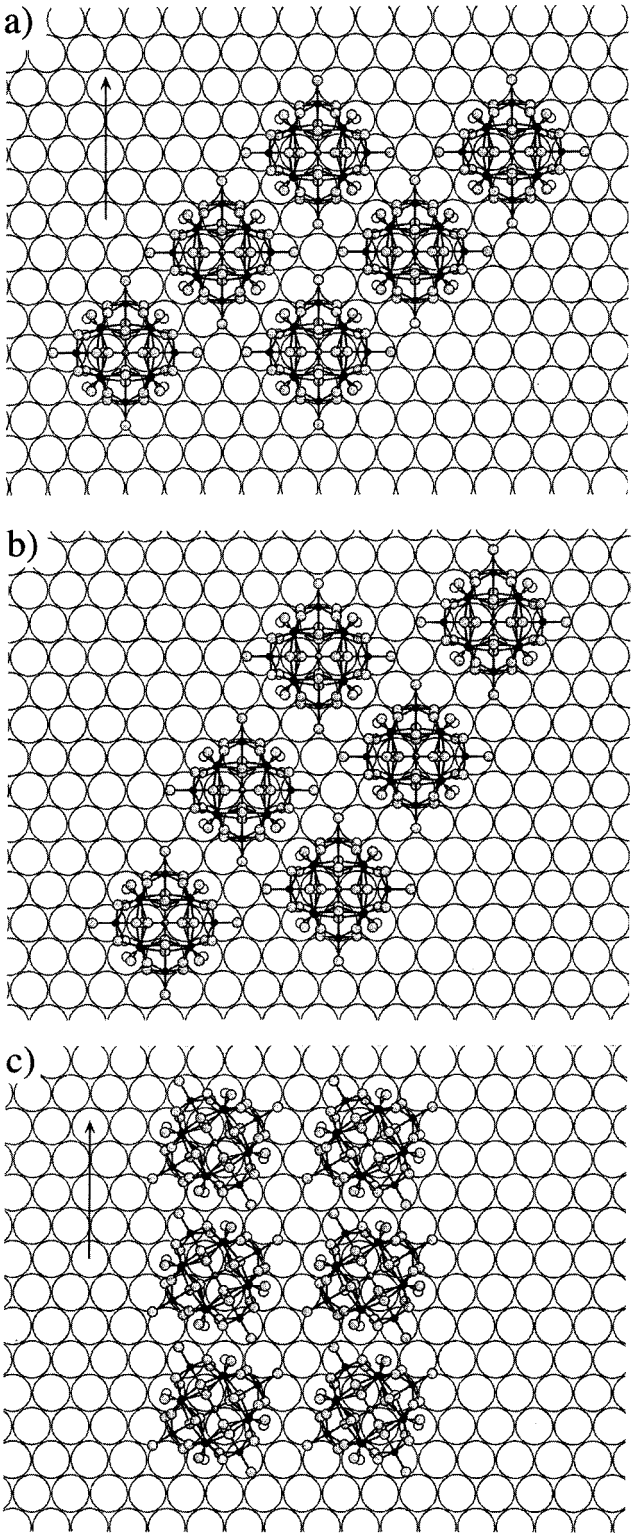

Figure 12. Proposed models for the (a) "square," (b) rhombic, and (c) row adlattices of the $SiW_{12}O_{40}^{4-}$ anion on Au(111). The arrow denotes the $\sqrt{3}$ direction on the Au-(111) surface in a and c. (Reprinted with permission from ref 33. Copyright 1997 Materials Research Society.)

on the metal surface: the rows in Figure 12c are parallel with the diagonals of the "square" unit cell in Figure 12a, and one of the sides of the diamond-shaped primitive cell ("square structure") in Figure 12a and the Au(111) metal surface rows intersect at 13.9°. In short, the observed structural parameters

are in good agreement with the values observed by STM.

VII. Toward the Future

In the context of modern surface science,[35,36] current understanding of polyoxanion surface chemistry is truly modest from a structural/mechanistic point of view. Nonetheless, this very same context gives enormous hope for the future in that most of the in situ surface analytical techniques available today have yet to be applied to polyoxoanion chemistry on solid surfaces. Only three techniques have received any attention to date, and none of them has been developed to anywhere near its full potential.

The quartz crystal microbalance (QCM) has been applied to the study of $SiW_{12}O_{40}^{4-}$, $H_2W_{12}O_{40}^{6-}$, and $P_2W_{18}O_{62}^{6-}$ adsorption on gold surfaces, both in the absence and presence of potential control.[37] Results obtained for the silicotungstate ion in the absence of potential control are consistent with the results of STM studies discussed above,[33] with rough estimates of surface coverage varying from 0.3 to 1.9 monolayers as silicotungstate ion concentrations were varied from 5×10^{-6} to 5×10^{-3} M. Imposition of a positive electrode potential of up to +0.5 V vs SCE failed to increase surface coverage beyond the levels observed at open circuit potential. This behavior is also consistent with high coverage, specific-anion adsorption of the type proposed for silicotungstate on gold on the basis of STM studies (see above). Quantitative interpretation of QCM experiments for adsorbed ions is difficult in the absence of supporting data, but QCM studies have already proven to be a useful qualitative tool for in situ monitoring of polyoxoanion adsorption and adsorption kinetics.[37]

A second technique that has shown great potential for in situ study of polyoxoanion surface chemistry at solid−liquid interfaces is modulated infrared spectroscopy.[38] Conventional infrared absorption experiments performed in either transmission or internal reflection mode probe not only the chemical species specifically adsorbed at the solid surface but also the species present in solution at distances of about up to about 1 μm from the surface. This presents great difficulties in distinguishing between absorption bands arising from species adsorbed on the surface and absorption bands arising from species present in the solution. In the case of electrolytes such as polyoxometalates, attempts have been made to circumvent these difficulties by varying the potential imposed on the surface and observing how infrared band intensities vary as a function of potential. To date, only one system involving early transition metal polyoxometalates has been investigated in this fashion: *n*-doped Ge in aqueous $H_4SiW_{12}O_{40}$.[38] Extensions to other types of modulation such as polarization modulation are likely to yield important information concerning fast kinetics and equilibria at the solid−liquid interface, information that is difficult or impossible to obtain by other means.

The third and final in situ surface analytical technique that has shown great promise but is yet to be exploited to its full potential is scanning probe microscopy. Both AFM and STM are capable of spatial resolution at the atomic level,[11] yet all studies of polyoxoanion surfaces reported to date have failed to achieve spatial resolution less than 10 Å. As a result, SPM has yielded useful structural information only when ordered arrays of polyoxoanion can be observed, and the only information thus obtained consists of two-dimensional unit cell parameters and, in some cases, unit cell orientations (see above). All evidence for polyoxoanion surface structure in terms of atomic arrangement within individual polyoxoanions therefore indirect and, to a certain extent, suspect. The challenge is clear: if polyoxoanion surface chemistry is to be understood at the same level of sophistication already achieved for polyoxoanions in solution and the solid state, then SPM image quality must be significantly improved. What are the prospects for the future? If the remarkable rate of improvement in image quality obtained between 1991 (Figure 3a) and 1996 (Figures 7 and 9a) can be maintained, it will not be long before the groups of atoms defining functional groups on polyoxoanion surfaces can be identified. When that time comes, polyoxoanion surface chemistry will indeed move toward the future, joining ranks with polyoxoanion chemistry in solution and the solid state.

VIII. Acknowledgments

This work was supported by the U.S. Department of Energy, Division of Materials Science grant DEFG02-96ER45439 through the University of Illinois at Urbana−Champaign, Frederick Seitz Materials Research Laboratory. The authors are deeply indebted to Professor Andy Gewirth for assistance in preparing this review.

IX. References

(1) Evans, H. T., Jr. *Perspect. Struct. Chem.* **1971**, *4*, 1.
(2) (a) Pope, M. T. *Heteropoly and Isopoly Oxometalates*; Springer: New York, 1983. (b) Day, V. W.; Klemperer, W. G. *Science* **1985**, *228*, 533.
(3) (a) Mizuno, N.; Misono, M. *Chem. Rev.* **1998**, *98*, 199 (this issue). (b) Okuhara, T.; Mizuno, N.; Misono, M. *Adv. Catal.* **1996**, *41*, 113. (c) Izumi, Y.; Urabe, K.; Onaka, M. *Zeolite, Clay, and Heteropoly Acid in Organic Reactions*; VCH: Weinheim, 1992.
(4) (a) Lomakina, S. V.; Shatova, T. S.; Kazansky, L. P. *Corros. Sci.* **1994**, *36*, 1645 and references therein. (b) Katsoulis, D. E. *Chem. Rev.* **1998**, *98*, 359 (this issue).
(5) (a) Sadakane, M.; Steckhan, E. *Chem. Rev.* **1998**, *98*, 219 (this issue). (b) Keïta, B.; Nadjo, L. *Mater. Chem. Phys.* **1989**, *22*, 77. (c) Rong, C.; Anson, F. C. *Anal. Chem.* **1994**, *66*, 3124. (d) Rong, C.; Anson, F. C. *Inorg. Chim. Acta* **1996**, *242*, 11.
(6) Lin, Y.; Finke, R. G. *J. Am. Chem. Soc.* **1994**, *116*, 8335.
(7) Srinivas, R. A.; Rosen, A.; Heller, A. *J. Electrochem. Soc.* **1993**, *140*, 3021.
(8) Kudo, T.; Ishikawa, A.; Okamoto, H.; Miyauchi, K.; Murai, F.; Mochiji, K.; Umezaki, H. *J. Electrochem. Soc.* **1987**, *134*, 2607.
(9) Yoshimura, T.; Ishikawa, A.; Okamoto, H.; Miyazaki, H.; Sawada, A.; Tanimoto, T.; Okazaki, S. *Microelectron. Eng.* **1991**, *14*, 149.
(10) Keïta, B.; Nadjo, L. *Surf. Sci. Lett.* **1991**, *254*, L443.
(11) Wiesendanger, R. *Scanning Probe Microscopy and Spectroscopy*; Cambridge University Press: Cambridge, 1994.
(12) Wiesendanger, R. *Scanning Probe Microscopy and Spectroscopy*; Cambridge University Press: Cambridge, 1994; pp 99−106 and 537−539.
(13) Wiesendanger, R. *Scanning Probe Microscopy and Spectroscopy*; Cambridge University Press: Cambridge, 1994; pp 97 and 537−539.
(14) Wiesendanger, R. *Scanning Probe Microscopy and Spectroscopy*; Cambridge University Press: Cambridge, 1994; pp 148−157 and 572.
(15) Sautet, P. *Chem. Rev.* **1997**, *97*, 1097.

(16) Keïta, B.; Nadjo, L.; Kjoller, K. *Surf. Sci. Lett.* **1991**, *256*, L613.
(17) Keïta, B.; Chauveau, F.; Théobald, F.; Bélanger, D.; Nadjo, L. *Surf. Sci.* **1992**, *264*, 271.
(18) Iball, J.; Low, J. N.; Weakley, T. J. R. *J. Chem. Soc., Dalton Trans.* **1974**, 2021.
(19) Song, I. K.; Kaba, M. S.; Coulston, G.; Kourtakis, K.; Barteau, M. A. *Chem. Mater.* **1996**, *8*, 2352.
(20) Brown, G. M.; Noe-Spirlet, M.-R.; Busing, W. R.; Levy, H. A. *Acta Crystallogr., Sect. B* **1977**, *33*, 1038.
(21) Jansen, S. A.; Singh, D. J.; Wang, S.-H. *Chem. Mater.* **1994**, *6*, 146.
(22) Kulesza, P. J.; Faulkner, L. R.; Chen, J.; Klemperer, W. G. *J. Am. Chem. Soc.* **1991**, *113*, 379.
(23) Watson, B. A.; Barteau, M. A.; Haggerty, L.; Lenhoff, A. M.; Weber, R. S. *Langmuir* **1992**, *8*, 1145.
(24) Song, I. K.; Kaba, M. S.; Barteau, M. A. *J. Phys. Chem.* **1996**, *100*, 17528.
(25) Kaba, M. S.; Song, I. K.; Barteau, M. A. *J. Phys. Chem.* **1996**, *100*, 19577.
(26) Kaba, M. S.; Song, I. K.; Barteau, M. A. *J. Vac. Sci. Technol. A* **1997**, *15*, 1299.
(27) A referee has cited circumstantial evidence in support of monolayer formation on graphite. In ref 19, the authors suggest that little or no water of crystallization is present in the arrays formed from aqueous $H_3PMo_{12}O_{40}$, $H_4PMo_{11}VO_{40}$, and $H_8PMo_{10}VCuO_{40}$ solutions by evaporative deposition on graphite, since the anion−anion separations observed in STM images of these arrays are nearly the same in all three cases. They contrast this behavior with that "expected" for bulk compounds, where "the eight protons in $H_8PMo_{10}VCuO_{40}$ would be expected to bind more water molecules than the four protons in $H_4PMo_{11}VO_{40}$." The authors' expectations are amply supported by precedent, yet counterexamples can be found in crystallographic data tabulated by Evans in ref 1. For example, $H_3PW_{12}O_{40}$, $H_4SiW_{12}O_{40}$, and $H_8W_{12}O_{40}$ can all form cubic Pn3m crystals containing 5 (to 6^{20}) water molecules of crystallization per anion, and the anion−anion separations determined X-ray crystallographically are nearly the same in all three cases.
(28) Hashimoto, M.; Misono, M. *Acta Crystallogr., Sect. C* **1994**, *50*, 231.
(29) Gewirth, A. A.; Niece, B. K. *Chem. Rev.* **1997**, *97*, 1129.
(30) (a) Keïta, B.; Nadjo, L. *J. Electroanal. Chem.* **1993**, *354*, 295. (b) Nadjo, L.; Keïta, B. *J. Phys. IV* **1994**, *4* (C1), 329.
(31) Zhang, B.; Wang, E. *J. Electroanal. Chem.* **1995**, *388*, 207.
(32) Ge, M.; Zhong, B.; Klemperer, W. G.; Gewirth, A. A. *J. Am. Chem. Soc.* **1996**, *118*, 5812.
(33) Ge, M.; Niece, B. K.; Wall, C. G.; Klemperer, W. G.; Gewirth, A. A. *Mater. Res. Soc. Symp. Proc.* **1997**, *451*, 99.
(34) Ge, M.; Gewirth, A. A.; Klemperer, W. G.; Wall, C. G. *Pure Appl. Chem.* **1997**, *69*, 2175.
(35) Masel, R. I. *Principles of Adsorption and Reaction on Solid Surfaces*; Wiley: New York, 1996.
(36) Somorjai, G. A. *Introduction to Surface Chemistry and Catalysis*; Wiley: New York, 1994.
(37) Keïta, B.; Nadjo, L.; Bélanger, D.; Wilde, C. P.; Hilaire, M. *J. Electroanal. Chem.* **1995**, *384*, 155.
(38) Chazalviel, J.-N.; Dubin, V. M.; Mandal, K. C.; Ozanam, F. *Appl. Spectrosc.* **1993**, *47*, 1411.

CR9603993